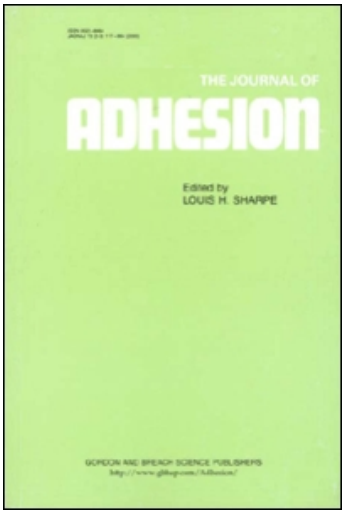


**The Journal of Adhesion**
Publication details, including instructions for authors and subscription information:
http://www.informaworld.com/smpp/title~content=t713453635

# Fundamentals of Adhesion Failure for a Model Adhesive (PMMA/Glass) Joint in Humid Environments

K. T. Tan[a]; C. C. White[a]; D. L. Hunston[a]; C. Clerici[a]; K. L. Steffens[b]; J. Goldman[a]; B. D. Vogt[c]
[a] Materials and Construction Research Division, National Institute of Standards and Technology (NIST), Gaithersburg, Maryland, USA [b] Process Measurements Division, National Institute of Standards and Technology (NIST), Gaithersburg, Maryland, USA [c] Department of Chemical Engineering, Arizona State University, Tempe, Arizona, USA

**To cite this Article** Tan, K. T. , White, C. C. , Hunston, D. L. , Clerici, C. , Steffens, K. L. , Goldman, J. and Vogt, B. D.(2008) 'Fundamentals of Adhesion Failure for a Model Adhesive (PMMA/Glass) Joint in Humid Environments', The Journal of Adhesion, 84: 4, 339 — 367
**To link to this Article: DOI:** 10.1080/00218460802004428
**URL:** http://dx.doi.org/10.1080/00218460802004428

*The Journal of Adhesion*, 84:339–367, 2008
ISSN: 0021-8464 print/1545-5823 online
DOI: 10.1080/00218460802004428

Taylor & Francis
Taylor & Francis Group

# Fundamentals of Adhesion Failure for a Model Adhesive (PMMA/Glass) Joint in Humid Environments

**K. T. Tan[1], C. C. White[1], D. L. Hunston[1], C. Clerici[1], K. L. Steffens[2], J. Goldman[1], and B. D. Vogt[3]**
[1]Materials and Construction Research Division, National Institute of Standards and Technology (NIST), Gaithersburg, Maryland, USA
[2]Process Measurements Division, National Institute of Standards and Technology (NIST), Gaithersburg, Maryland, USA
[3]Department of Chemical Engineering, Arizona State University, Tempe, Arizona, USA



*The origins for the abrupt adhesion loss at a critical relative humidity (RH) for polymeric adhesives bonded to inorganic surfaces were explored using a poly-(methyl methacrylate) (PMMA) film on silicon oxide as a model system. The interfacial and bulk water concentrations within the polymer film were quantified as a function of $D_2O$ partial pressure using neutron reflectivity. The adhesive fracture energies of these PMMA/$SiO_2$ interfaces at the same conditions were determined using a shaft-loaded blister test. Discontinuities in the adhesive fracture energy, bulk moisture solubility, and the width of the interfacial moisture excess near the interface were observed at the critical RH. A mechanism based on the coupling of bulk swelling-induced stresses with the decreased cohesive strength due to moisture accumulation at the interface is proposed and is consistent with all experimental observations.*

**Keywords:** Critical RH; Critical water content; Durability; Fracture mechanics; Mechanisms; PMMA/glass interface

Received 5 November 2007; infinal form 7 February 2008.
One of a Collection of papers honoring John F. Watts, the recipient in February 2008 of *The Adhesion Society Award for Excellence in Adhesion Science, Sponsored by 3M*.

Address correspondence to Kar Tean Tan, Polymeric Materials Group, Building and Fire Research Laboratory, National Institute of Standards and Technology, 100 Bureau Drive, Stop 8615, Gaithersburg, MD 20899-8615, USA. E-mail: kar.tan@nist.gov and Bryan D. Vogt, Department of Chemical Engineering, Arizona State University, Tempe, AZ 85281, USA. E-mail: bryan.vogt@asu.edu

## 1. INTRODUCTION

Significant growth in the use of polymeric adhesives has emerged in recent years, especially in technically demanding applications. The driving force for the continual growth of adhesives in engineering applications is the many advantages that adhesives offer over the more traditional methods of joining such as welding, riveting, brazing, mechanical fasteners, etc. [1]. These advantages include more uniform stress distributions, improved fatigue resistance, increased design flexibility, decreased production expenses, and lower maintenance costs. However, several issues have limited the wider application of adhesives. One of the most important issues is the lack of knowledge concerning the durability of adhesive joints upon exposure to moisture. Moisture-induced adhesion loss is a significant problem in long-term viability of many products. Despite the wealth of data in the literature for adhesion failure in humid environments, the mechanisms of moisture-induced adhesion loss are not entirely understood. The presence of moisture in adhesive joints may not only weaken the physical and chemical properties of a bulk adhesive itself (*via* plasticization [2–4], swelling [5–7], and degradation [8,9]), but also the interface between the adhesive and the substrate. Water at the interface has been hypothesized to be the primary cause of adhesion loss for many adhesive systems. The primary effects of water at the interface include hydrolysis of secondary interfacial bonds [10,11], hydration of oxide structure of the substrate [12–14], and cathodic delamination [10,15,16].



The influence of water on adhesion loss is generally strongly dependent upon the ambient humidity. For some adhesive systems, there appears to be a critical humidity level below which minimal changes in adhesive strength occur over a relatively long time-scale [13,17,18]. However, if the humidity exceeds that of the critical level, the adhesive fails catastrophically with no prior warning. This raises serious questions on the safety aspects of such adhesive systems for significant load-bearing engineering applications. Therefore, fundamental understanding of this rapid adhesion loss occurring at a critical relative humidity is important to the adhesive industry. While these adhesion losses have been studied, the underlying mechanisms remain poorly understood. Brewis *et al*. [13], for example, attributed the sudden change in adhesive strength at the critical humidity for an epoxy/aluminum system to hydration of the metal oxide substrate. Conversely, Lefebvre *et al*. [17] explained this sudden change for an epoxy/glass system by a completely different mechanism involving hydroxyl groups that are present throughout the adhesive, so bulk

adhesive properties are important. An improved understanding of the mechanism for adhesion loss at and above a critical relative humidity (RH), therefore, would be tremendously useful for development of rational strategies to improve adhesion performance. The aim of the present study is to address this issue. We chose a simple adhesive system consisting of poly(methyl methacrylate) (PMMA) adhered to a glass surface investigated over a wide range of RH from 0 to 100% at $23 \pm 0.2^{\circ}C$. A fracture mechanics approach is used to investigate adhesive failure. In addition, the loci of joint failure have been assessed using attenuated total-reflection FTIR and XPS. A key aspect of this study is the use of neutron reflectivity to provide the distribution of water within the model adhesive as a function of humidity. In tandem, these metrologies enable an improved picture of the underlying mechanisms of adhesive failure in humid environments.



## 2. EXPERIMENTAL[§]

### 2.1. Materials and Joint Preparation

For adhesive joint testing, the substrate was a 3.2 mm thick borosilicate glass (Swiftglass, Elmira, NY, USA) with an 8 mm diameter hole bored through its center. The bulk composition of the glass is provided in Table 1. The PMMA has $M_w = 1.2 \times 10^5$ g/mol. Prior to bonding, each substrate was rigorously cleaned using acetone. The specimen was multi-layered as depicted in the schematic illustration shown in Fig. 1 and prepared as follows. First, a pre-crack was fabricated by placing a 0.95 cm diameter piece of Kapton® (Dupont Electronic Technologies, Circleville, OH) pressure sensitive adhesive tape (PSAT) over the hole in the center of the substrate. The Kapton® PSAT consists of a 25 μm thick Kapton® backing and a 37.5 μm thick acrylic pressure sensitive adhesive. A nominally 15 μm thick PMMA film was spin coated at a speed of 104.7 rad/s for 20 s from 15% mass fraction solution of PMMA in toluene. On top of the PMMA, an epoxy mixture consisting of bisphenol-A based epoxy resin and Jeffamine T-403 curing agent (43 parts per hundred of epoxy resin) (Huntsman, The Woodlands, TX, USA) was spin-coated at 104.7 rad/s for 20 s. No solvent was added to the epoxy mixture. A 50 μm thick piece of Kapton® film was then placed on top of the uncured epoxy resin to act as a mechanical reinforcing layer for the PMMA coating. The composite adhesive was cured at room

[§]Certain commercial products or equipment are described in this article in order to adequately specify the experimental procedure. In no case does such identification imply recommendation or endorsement by the National Institute of Standards and Technology (NIST), nor does it imply that it is necessarily the best available for the purpose.

**TABLE 1** Bulk Composition of the Borosilicate Glass (Data from the Manufacturer)

| Materials | Chemical formula | Composition (mass %) |
|---|---|---|
| Sand | $SiO_2$ | 81 |
| Alumina | $Al_2O_3$ | 2 |
| Soda ash | $Na_2O/K_2O$ | 4 |
| Boric oxide | $B_2O_3$ | 13 |

temperature for 48 h after which it was cured at 60°C for 1 h. The resulting adhesive layer was, therefore, a multi-layered composite consisting of the pre-crack Kapton® PSAT, PMMA, epoxy resin, and Kapton® film.

## 2.2. Environmental Preconditioning

The joints were preconditioned at a constant RH of 2, 25, 42.5, 50, 60, 62.5, 65.1, 68.5, 70, 85, and 100 ± 2% RH for 72 h at room temperature, approximately 23 ± 0.2°C. The RH was regulated within a Tenney temperature humidity chamber (Tenney, New Columbia, PA, USA). It should be noted that water uptake in bulk PMMA had reached saturation in each environment prior to testing, so there was no gradient in concentration in the joints. Elapsed time between removal of the joints from the chamber and testing was less than 5 min. The joints were tested at ambient conditions, nominally 23°C and 25% RH. Since only one aging time was used, the time-dependent environmental effect after saturation has not been measured, although such phenomena



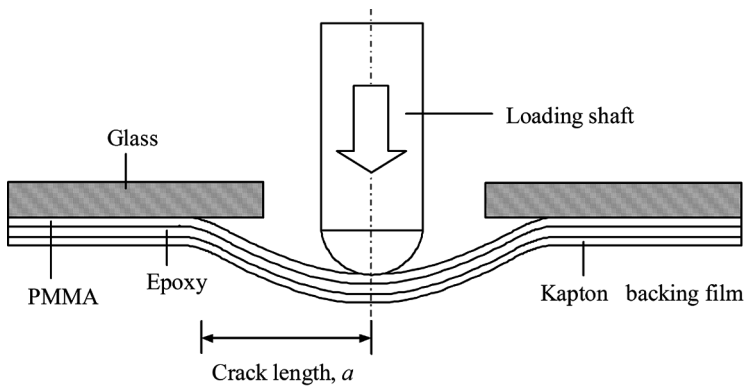


**FIGURE 1** Schematic of the shaft-loaded blister test joint (not to scale). The arrow indicates the direction of loading.

may exist [19]. However, within the time-frame of the present experiment, such a time-dependent environmental effect was not observed.

## 2.3. Material Characterization

### 2.3.1. Fracture Mechanics Tests

The joints were tested with a shaft-loaded blister test using a screw-driven tensile testing machine (MTS, Eden Prairie, MN, USA) at a cross-head displacement rate of 5 μm/s. The adhesive fracture energy, $G_C$, was calculated from the load based equation [20]:

$$G_C = \left(\frac{1}{16\pi^4 Eh}\right)^{\frac{1}{3}} \cdot \left(\frac{P}{a}\right)^{\frac{4}{3}}, \tag{1}$$

where $P$ is the load, $a$ is the crack length, $E$ is the Young's modulus, and $h$ is the total thickness of the composite layer. The modulus of the laminate was estimated using the rule of mixtures [21]:

$$E = \sum_{i=0}^{i} \upsilon_i E_i, \tag{2}$$

where $E_i$ and $\upsilon_i$ are the modulus and volume fraction of the $i$th component, respectively. Note that the mechanical properties of the laminate may be affected upon moisture absorption. Because of relatively good water resistance of the Kapton® films, the effect of water on their mechanical properties is considered minimal within the time-scale of the present experiment. In contrast, the epoxy and PMMA are highly susceptible to moisture absorption affecting their mechanical properties. However, it should be noted that moisture absorption has little effect on the measured $G_C$ because it depends weakly on modulus and thickness changes, *i.e.*, $G_C \sim (1/Eh)^{1/3}$. The insensitivity to changes in modulus and thickness makes the shaft-loaded blister test particularly advantageous for durability studies [21]. Thus, the moduli for the PMMA, epoxy, and Kapton films were assumed constant, and were approximately 3.3 GPa [22], 6 GPa [21], and 2.5 GPa [21], respectively. Joints were tested in triplicate at each RH.

### 2.3.2. Examination of the Fracture Surfaces

FTIR was utilized to characterize the fracture surfaces. References for the pure materials (glass substrate, PMMA, and epoxy) were used for comparison with the failure surfaces. Infrared analysis was carried out using a Nicolet Nexus FTIR Spectrometer (Nicolet, Ramsey, MN, USA) equipped with a mercury-cadmium-telluride detector and a

SensIR Durascope ATR accessory (SensIR Technologies, Danbury, CT, USA). Dry air was used as the purge gas. Consistent pressure on the specimens was applied using the force monitor on the Durascope, and the sampling area was approximately 1 mm in diameter. All spectra were collected in the range from 650 to 4000 $cm^{-1}$ at a nominal resolution of 4 $cm^{-1}$, and averaged over 132 scans. Five different locations on each specimen were analyzed. Note that it is not always possible to determine with certainty the locus of failure using ATR-FTIR since the penetration depth of an ATR-FTIR evanescent wave is on the micron scale [23]. XPS was also employed to provide better resolution for thin residual films using a Kratos Axis Ultra DLD spectrometer (Kratos, Chestnut Ridge, NY, USA). Monochromatic aluminum $K_\alpha$ set to a spot size of $300 \times 700$ μm was used as the x-ray source. Survey spectra were performed with a pass energy of 160 eV to detect all peaks, which was followed by a high-resolution examination using a pass energy of 40 eV.



### 2.3.3. Water Sorption Isotherm Measurement

The water sorption-desorption isotherms were measured at $23 \pm 0.1$°C using a moisture sorption analyzer equipped with a microbalance having a mass resolution of 0.1 μg (Hiden Analytical, Warrington, UK). The instrument can accurately control the environmental chamber to within ±0.5% of the preset values of RH for the entire RH range of the present study. Thick PMMA free-standing films ($5 \times 5 \times 0.55$ mm) were initially dried, then sorption and desorption isotherms were measured. Duplicate measurements indicated that the isotherm data were highly reproducible. Water sorption and desorption isotherms for PMMA were analyzed using the Guggenheim-Anderson-de Boer (GAB) model, which has been shown to be suitable for describing water sorption isotherms of a variety of polymers over a wide RH range [24,25]:

$$m_{a_w} = \frac{mCka_w}{(1 - ka_w)} \cdot \frac{1}{1 + (C - 1)ka_w}, \tag{3}$$

where $C$ is the GAB constant, $m$ is the monolayer water content corresponding to the amount of sorbed water necessary to form a monolayer, $a_w$ is the water activity (*i.e.*, RH/100), and $k$ is a correcting factor typically less than 1. To determine these parameters, the GAB equation is linearized to the following expression:

$$f = \frac{a_w}{(1 - ka_w)m_{a_w}} = \frac{1}{Cmk} + \frac{(C - 1)}{Cm} \cdot a_w. \tag{4}$$

The plot of $f$ *versus* $a_w$ within the range of $0.1 < a_w < 0.8$ should produce a straight line if a reasonable value for $k$ is used. The intercept and slope of the line are $\frac{1}{Cmk}$ and $\frac{(C-1)}{Cm}$, respectively, allowing the determination of the GAB parameters, $C$ and $m$.

### 2.3.4. Contact Angle Measurement

Contact angles formed by droplets of distilled water were measured on glass substrates and PMMA surfaces using the sessile drop method, employing a 'Ramè-Hart A-100' goniometer (Ramè-Hart, Netcong, NI, USA).

### 2.3.5. Neutron Reflectivity (NR) Experiment

Specimens for NR were prepared on silicon wafers with a thermal oxide layer. This oxide layer "mimics" the glass utilized in the adhesion measurements. Thin films of PMMA were spin coated on the silicon wafer. Deuterium oxide (Sigma-Aldrich, 99.9% pure, Aldrich, St. Louis, MO, USA) was utilized to enable direct quantification of the water distribution within the film as a function of the partial pressure (humidity) of $D_2O$. NR measurements were performed at the Center for Neutron Research on the NG-7 reflectometer at the National Institute of Standards and Technology (NIST) (Gaithersburg, MD, USA) in the following configuration: wavelength $(\lambda) = 4.768$ Å and wavelength spread $(\Delta\lambda/\lambda) = 0.025$. NR is capable of probing the neutron scattering density at depths of up to several thousand Å, with an effective depth resolution of several Å.



## 3. RESULTS AND DISCUSSION

### 3.1. Adhesion in Dry and Humid Environments

The dependence of $G_C$ on RH is shown in Fig. 2. At low humidity levels below 50% RH, the $G_C$ values were relatively high and were statistically independent of RH, indicating that the joints exhibited good adhesion. In these cases, the crack propagated in an unstable, stick-slip manner with crack initiation followed by fast crack growth, and then crack arresting. A load-displacement curve for such crack growth shows a characteristic saw-tooth appearance. The peak values of the load represent the load for the onset of crack growth and the average of these values was used to determine the value of $G_C$. The locus of joint failure was always visually cohesive through the polymer layer. In this RH range, moisture has been found not to affect the $G_C$ values.

A transition in behavior is observed for RH between 60 and 68%. Analogous stick-slip crack propagation is observed, but the $G_C$ values

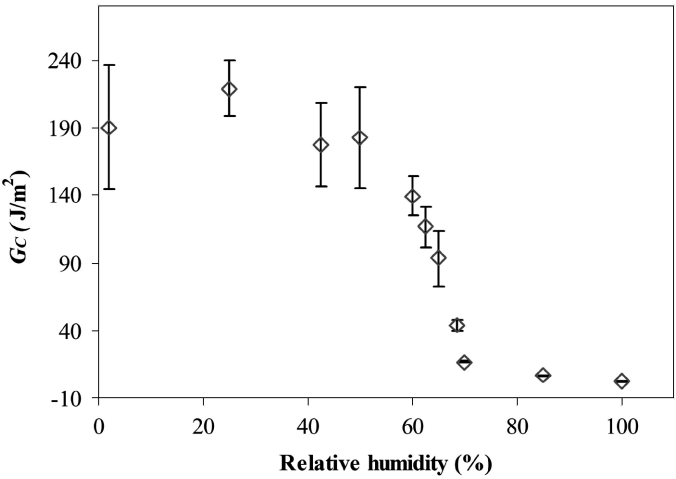


**FIGURE 2** The impact of RH on $G_C$ of the PMMA/glass joint. The fracture energy is determined from shaft-loaded blister tests conducted at $23 \pm 2$°C. The error bars represent plus or minus one standard deviation from the mean value.



rapidly decreased by nearly two orders of magnitude. This transition is accompanied by a complex failure path involving both cohesive failure within the polymer layer and truly interfacial failure along the polymer/oxide interface. Therefore, there appears to be a critical concentration of water below which the environment has a minimal impact on the failure. Similar observations have been made in epoxy/aluminum joints [13], epoxy/glass joints [17,26], and epoxy/mild steel joints [27,28]. The presence of critical water concentration in thermoplastic-based adhesives has not been previously reported in the literature. For all these systems, the critical RHs usually fall into the range between 60 and 80%, depending on an adhesive/substrate system; variations result from specific chemistries and their interactions with moisture.

At higher RH (>68%), the crack grew in a stable manner visually along the polymer/oxide interface. The $G_C$ values were extremely low, indicating gross deterioration of adhesion between the PMMA and glass at elevated humidity levels. The adhesive strength of the interface decreases slowly as the RH is increased further. However, for all cases at RH > 68%, the strength of the joint is extremely poor. A visual assessment of the failure surfaces, however, does not reveal exactly the locus of joint failure, therefore ATR-FTIR and XPS

analyses have been conducted and the results will be presented in the next section.

## 3.2. The Loci of Joint Failure

The failure location of the joint provides insight into the mechanism by which it is degraded by moisture. In any assessment of the locus of joint failure, it is essential to establish the condition of the surfaces prior to the bonding process. Figure 3 shows the ATR-FTIR spectra for these "control" surfaces: glass substrate, PMMA, and epoxy. The primary peaks in the spectrum of PMMA include 2950 $cm^{-1}$ ($-CH_3$ asymmetric stretching), 1725 $cm^{-1}$ (C=O stretching), 1450 $cm^{-1}$ ($C-CH_3$ asymmetric deformation coupled with $O-CH_3$ deformation), and 1147 $cm^{-1}$ (asymmetric C–O–C stretching) [23]. Siloxanes of the glass substrate were characterized by a strong band centered at 1000 $cm^{-1}$ due to the Si–O–Si asymmetric stretching. Note that



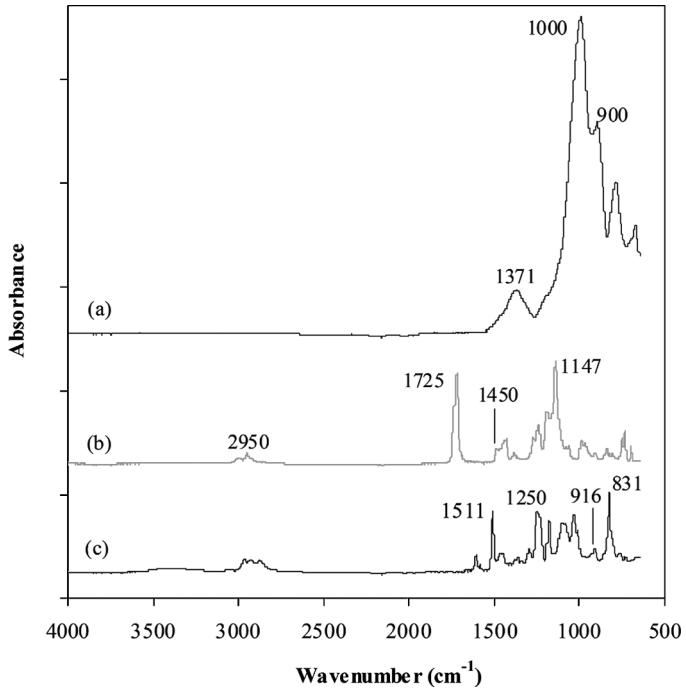


**FIGURE 3** ATR-FTIR spectra for control surfaces: (a) glass substrate, (b) PMMA, and (c) epoxy. These are utilized as references for the fracture surfaces.

normal atmospheric exposure always results in glass ($SiO_2$) surfaces covered with silanol (Si−OH) groups, which are produced by the reaction of $SiO_2$ with ambient moisture [29]. Such silanol groups are identified by absorption at 900 $cm^{-1}$, which is attributed to the Si−O stretching [23]. The presence of the boron in the glass is clearly visible from an intense absorption at 1371 $cm^{-1}$, involving the stretching of the B−O bond [23]. Epoxy ring compounds absorb at 916 $cm^{-1}$ due to oxirane rings. Other strong absorption bands related to epoxy include 831 $cm^{-1}$ (out-of-plane bending of the p-disubstituted benzene ring), 1250 $cm^{-1}$ (aryl-O stretching), and 1511 $cm^{-1}$ (C=C stretching of the benzene ring) [30].

These spectra of the control specimens are then compared with those of the fracture surfaces to determine spectroscopically the loci of failure. ATR-FTIR spectra for joints preconditioned at 25% RH are shown in Fig. 4. Both glass and adhesive failure surfaces are spectroscopically similar to the control PMMA surface, indicating that



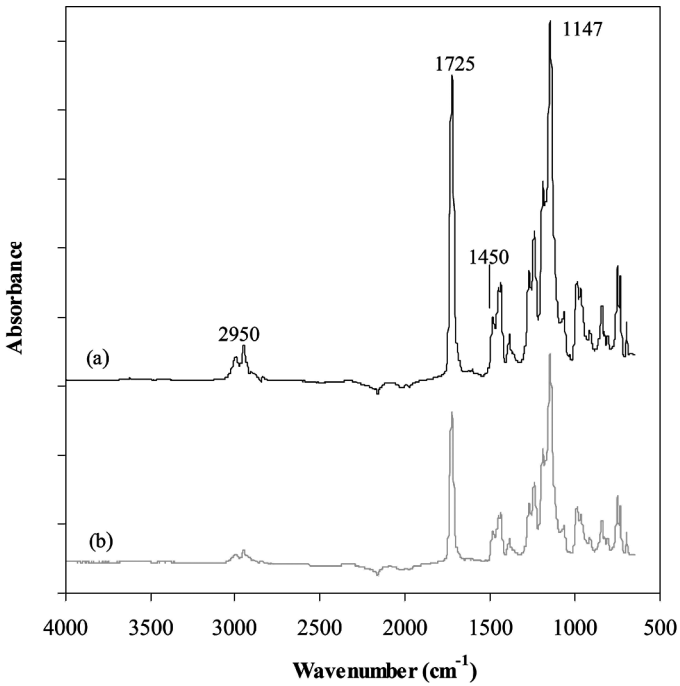


**FIGURE 4** ATR-FTIR spectra for joints preconditioned at 25% RH: (a) glass failure surface and (b) adhesive failure surface. Both surfaces appear to be predominately PMMA and thus it is concluded that the joint failed cohesively.

joint failure took place cohesively within the PMMA layer. Exposure to 65% RH results in the spectrum of the adhesive failure surface being always broadly similar to the control PMMA surface, and that for low RH specimens. However, the glass failure surfaces now show spectra similar to the control PMMA and control glass surface (Fig. 5) depending upon the location on the failure surface probed. This observation signifies that the locus of fracture is a mixture of interfacial failure along the PMMA/glass interface and cohesive failure within the PMMA layer. These data reinforce the conclusion that both interfacial failure and cohesive failure occur by the visual appearance of the glass failure surface. However, a different picture emerges when joints are preconditioned at 100% RH. The glass failure surface was very clean in visual inspection. The ATR-FTIR spectrum resembles the control



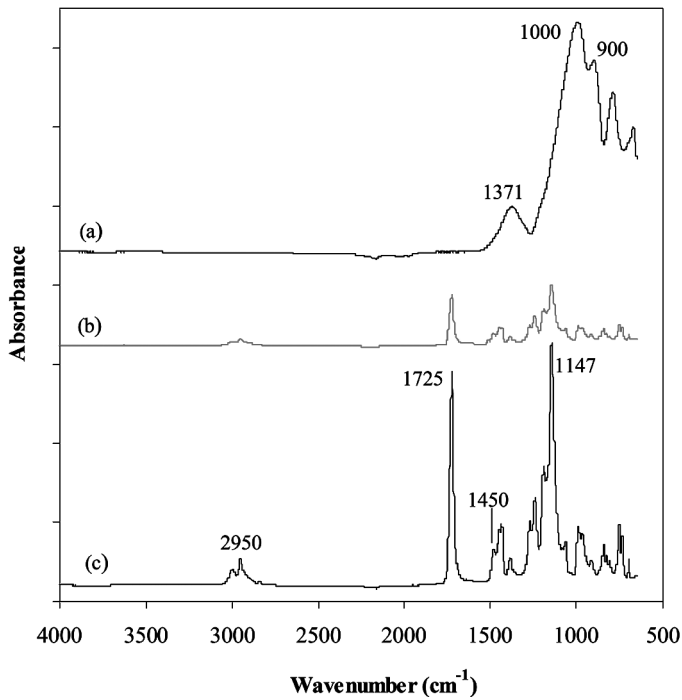


**FIGURE 5** ATR-FTIR spectra for joints preconditioned at 65% RH: (a) glass failure surface, (b) different location on glass failure surface, and (c) adhesive failure surface. The adhesive failure surface is always found to be PMMA, but the chemistry of the glass failure surface is location dependent. Either bare glass or PMMA appears to be at this later surface, indicating a combination of interfacial and cohesive failure.

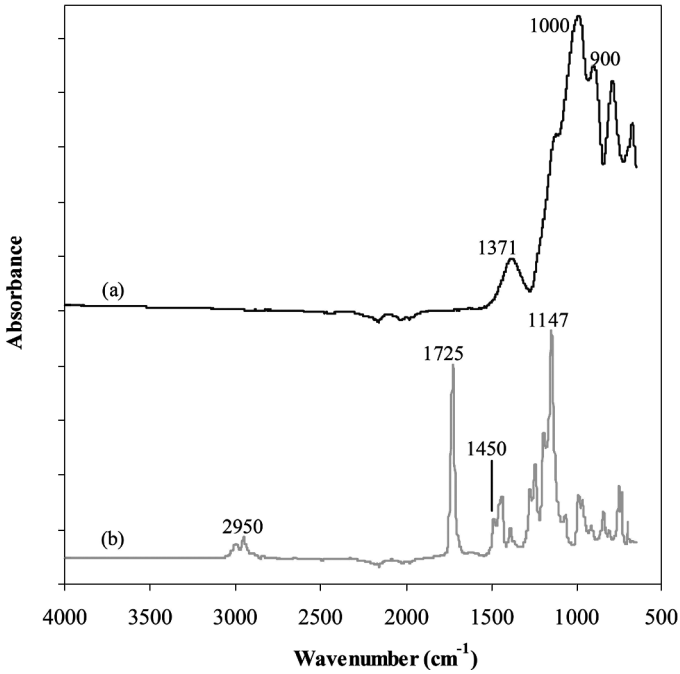


**FIGURE 6** ATR-FTIR spectra for joints preconditioned at 100% RH: (a) glass failure surface and (b) adhesive failure surface. The adhesive failure surface is PMMA, while the glass failure surface lacks the signature for PMMA. Thus, the failure is interfacial at 100% RH.



glass surface, as shown in Fig. 6. The spectrum of the corresponding adhesive failure surface is similar to the control PMMA, suggesting that the failure mode is predominantly interfacial. However, to ensure that joint failure had not occurred in a layer very close to the interface, which was too thin to be detected using the ATR-FTIR, XPS was utilized to characterize the fracture surfaces.

Similar to ATR-FTIR, XPS spectra for the control glass substrate, PMMA, and epoxy are necessary for ease of analysis of the fracture surfaces. The survey spectra and the elemental compositions for these surfaces are shown in Fig. 7 and Table 2, respectively. The glass surface has little adventitious carbon contamination, as indicated by the low C 1s signal. Strong silicon and oxygen photoelectron signals are consistent with the nominal composition of the borosilicate glass (Table 1). A peak corresponding to Sn 3d is visible and equates to a surface concentration of 0.03 atomic %. This tin signal is derived from the float-glass process, which involves melting glass and feeding a thin

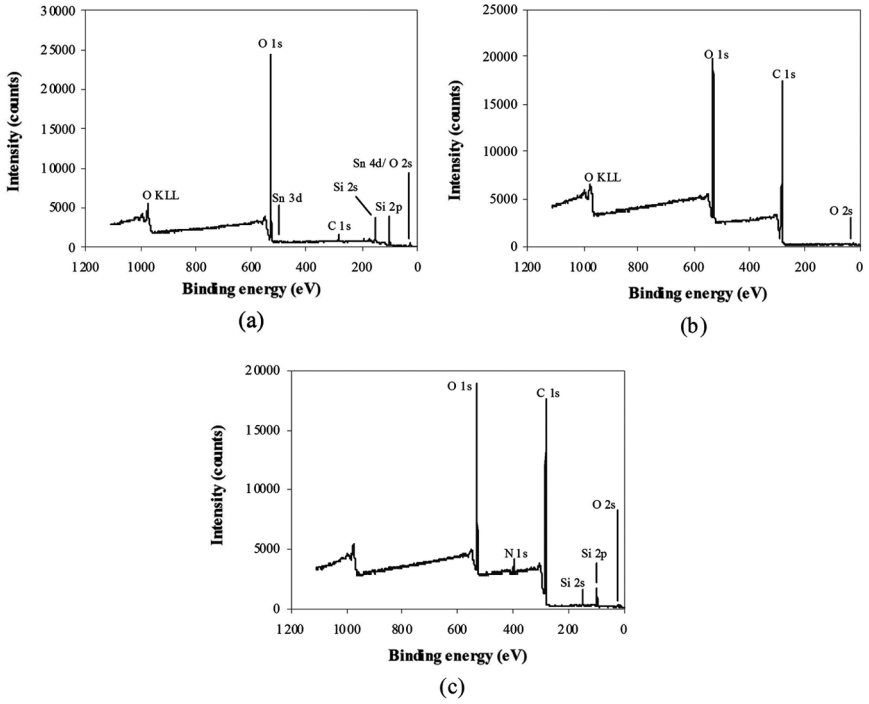


**FIGURE 7** XPS survey spectra for control surfaces: (a) glass substrate, (b) PMMA, and (c) epoxy. These are utilized as references for the fracture surfaces to determine the loci of failure.



layer of the molten glass onto a tank of molten tin, protected by an inert nitrogen atmosphere [31]. Subsequently, a glass surface inherently contains trace amounts of tin. This illustrates the high sensitivity of the XPS measurement which will be exploited when characterizing joint surfaces after failure. For the polymeric materials (PMMA and epoxy), high concentrations of oxygen and carbon are observed. Some nitrogen is present in the epoxy due to the amine curing agent. High resolution spectra for C 1 s region are also obtained for all samples (not shown). The C 1 s spectra for PMMA were fitted with three peaks corresponding to C–C or C–H carbon at 285.0 eV, C–O carbon at 286.7 eV, and O–C=O carbon at 288.8 eV. For the epoxy, the spectra consisted of two large peaks at 285 eV (C–C or C–H) and 286.7 eV (C–O). Thus, the relative concentrations of these carbon atoms in the epoxy and PMMA are unique due to their respective molecular structures; this provides unambiguous identification for the polymers.

**TABLE 2** Quantitative XPS Surface Analyses of the Control Specimens and Failure Surfaces

| Specimens | Surface composition (atomic %) | | | | | |
|---|---|---|---|---|---|---|
| | O | Sn | Na | N | C | Si |
| Glass substrate | 60.18 | 0.03 | 0.07 | 0.33 | 10.44 | 28.95 |
| PMMA control | 22.73 | – | – | 0.40 | 76.78 | 0.09 |
| Epoxy control | 17.47 | – | – | 2.47 | 75.21 | 4.85 |
| 25% RH | | | | | | |
| Glass failure surface | 23.52 | – | – | 0.31 | 75.54 | 0.63 |
| Adhesive failure surface | 21.69 | – | – | 0.34 | 77.86 | 0.11 |
| 65% RH | | | | | | |
| Glass failure surface | 56.95 | 0.83 | 0.11 | 0.92 | 15.29 | 25.9 |
| Adhesive failure surface | 15.14 | – | – | 5.15 | 78.13 | 1.58 |
| 100% RH | | | | | | |
| Glass failure surface | 51.15 | 0.58 | 0.08 | 0.98 | 22.68 | 24.53 |
| Adhesive failure surface | 14.85 | – | – | 4.67 | 79.09 | 1.39 |
| 100% RH (recovery) | | | | | | |
| Glass failure surface | 52.40 | 0.42 | 0.09 | 1.15 | 21.61 | 24.33 |
| Adhesive failure surface | 22.70 | – | – | 0.46 | 76.78 | 0.06 |



From comparison with control spectra similar to the ATR-FTIR described previously, the locus of failure for the preconditioned joints is determined utilizing XPS data. XPS survey spectra for the failure surfaces preconditioned at 25% RH are shown in Fig. 8. These spectra provide quantitative compositional information of the surfaces as shown in Table 2. The spectrum of the glass failure surface after preconditioning at 25% RH is very similar to the control PMMA surface

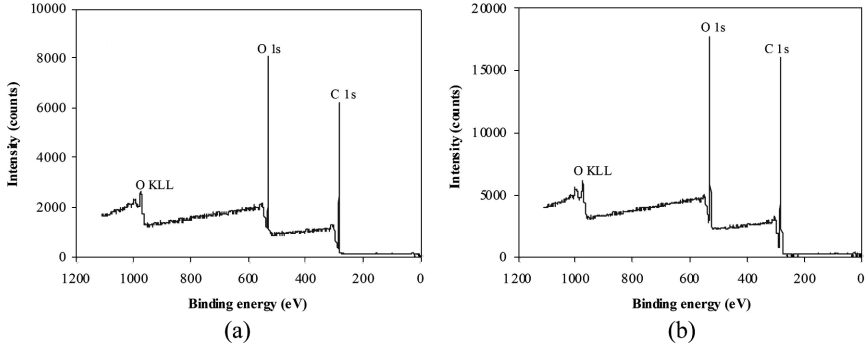


**FIGURE 8** XPS survey spectra for joints preconditioned at 25% RH: (a) glass failure surface and (b) adhesive failure surface. Both surfaces are consistent with PMMA, indicative of cohesive failure.

shown in Fig. 7(b) with no nitrogen detected. These observations collectively indicate that the failure mode is predominantly cohesive within the PMMA layer. This conclusion is further reinforced by the spectrum of the adhesive failure surface [Fig. 8(b)], showing that the adhesive failure surface is spectroscopically similar to that of the control PMMA [Fig. 7(b)]. The N 1 s signal is absent on the adhesive failure surface. There should be no epoxy residues at the interfacial region between the PMMA and glass substrate since the epoxy merely acts as an adhesive for bonding between the Kapton film and PMMA layer. This result is consistent with the high resolution spectra for C 1 s region (not shown) and previous ATR-FTIR measurements.

Previously the failure locus from the joint preconditioned at 100% RH was determined to be the interface between PMMA and glass both from visual inspection and ATR-FTIR. However, sensitivity limitations of ATR-FTIR could result in missing a small layer of PMMA remaining on the glass. To confirm the interfacial failure at 100% RH, XPS was utilized to characterize the joint failure surfaces. The spectra from both the glass and adhesive failure surfaces are shown in Fig. 9. The spectra from the adhesive failure surface are similar to that for the epoxy due to the presence of nitrogen at the surface. Also, the high resolution spectra for the C 1 s region indicate the presence of both epoxy and PMMA on the adhesive failure surface (not shown). This would suggest that failure occurred at the epoxy/PMMA interface. This is counter to the ATR-FTIR result. However, an alternative explanation for the presence of the nitrogen in the XPS spectra from the adhesive failure surface may be that moisture enables diffusion of



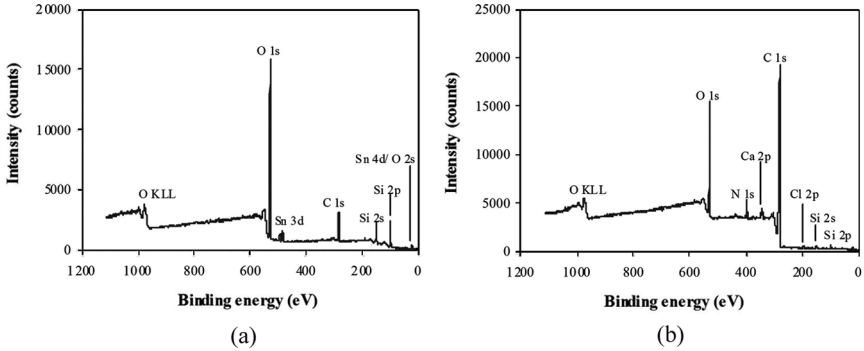


**FIGURE 9** XPS survey spectra for joints preconditioned at 100% RH: (a) glass failure surface and (b) adhesive failure surface. The glass failure surface is consistent with the glass control, thus the joint fails at the interface.

the amine in the epoxy into the PMMA. This conclusion is further supported by the XPS spectra for the glass failure surface, which resembles the original glass substrate. The carbon signal is only slightly elevated over the control indicating the amount of PMMA remaining on the surface is almost negligible. This result is consistent with the previous optical inspection and ATR-FTIR conclusion.

### 3.3. Isothermal Moisture Sorption Measurements

The results above are consistent with the interface playing a major role in the failure at the critical RH. Moreover, previous studies on the adhesion of PMMA to different surfaces in humid environments demonstrated that the failure mode at 100% RH at 23°C could be controlled between interfacial and cohesive through modification of the substrate surface energy [32]. Thus, one might conclude that interfacial moisture is responsible for the rapid drop in the strength of the adhesive joint near 65% RH.



The alternative mechanism is that bulk adhesive properties are important. The major supporting evidence for this mechanism is the observation of a deviation in bulk water solubility that occurs at the same RH where the drop in adhesive strength is found [17,26]. It would be strange for these two events to occur at the same RH and there could presumably be a connection between them. To assess any bulk effect on the PMMA system, moisture sorption was measured on bulk PMMA. Figure 10 illustrates the bulk water sorption-desorption isotherms for PMMA at 23°C for a range of RH from 5 to 95%. The sorption isotherms are shown in term of the mass of water sorbed at a given RH divided by the dry mass of the polymer. No error bars are given in those results because only one data point was recorded for each RH. However, as indicated earlier, the recording of moisture behaviors for all RH was highly reproducible. Based on the shape of the isotherm using the BET classification [33], PMMA-water behaves as Type III. The sorption isotherm represented by closed symbols shows that the water uptake increases linearly with increasing RH below the critical RH for adhesion loss determined from the fracture experiments. For higher RH, a deviation from Henry's law is observed with an upward curvature. The maximum moisture content is 1.12% for 94.5% RH. Sorption was followed by desorption over the same range of RH. A slight hysteresis, which decreases with decreasing RH, is observed. Figure 11 shows the magnitude of the hysteresis by giving the difference in moisture contents between sorption and desorption isotherms. The hysteresis is relatively small. A nearly constant and very small hysteresis is observed for the RH range

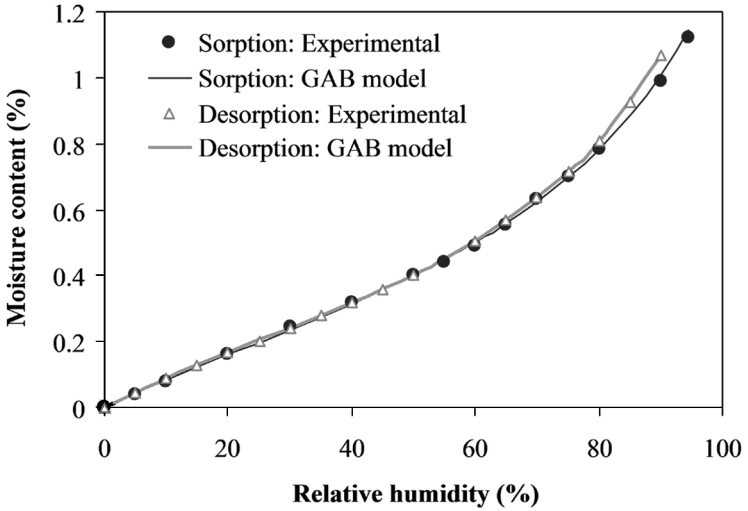


| Isotherm | $C$ | $m$ (%) | $k$ | RSS |
|---|---|---|---|---|
| Sorption | 3.054 | 0.392 | 0.74 | 0.000824 |
| Desorption | 3.476 | 0.357 | 0.78 | 0.001804 |

**FIGURE 10** PMMA moisture sorption (closed symbols) and desorption (open symbols) isotherms at 23°C. Note a kink in the isotherms at RH greater than 65%. The table provides the parameters obtained from fitting the sorption data to the GAB model.



below 60%; above this RH, the hysteresis increases continuously with increasing RH.

The diffusion coefficients of water (D) for moisture sorption and desorption in PMMA at 23°C are shown in Fig. 12 as a function of either the RH or water concentration. For RH $< 60\%$, the diffusivity of the water, $(5.2 \pm 0.3) \times 10^{-8}\,\mathrm{cm}^2/\mathrm{s}$, is constant and consistent between sorption and desorption. At higher RH, D becomes concentration-dependent where the water diffusivity decreases with increasing water concentration in the polymer. The upturn observed in the sorption-desorption isotherms and the decrease of diffusivity with concentration of sorbed water are indicative of cluster formation [34,35]. This phenomenon is usually explained by the fact that water molecules within a cluster are less mobile than an isolated molecule sorbed within the polymer matrix, and clustering causes an increase in the average size of the migrating water unit, thereby reducing D [34,35]. It is noteworthy that the deviation in diffusion coefficients and moisture

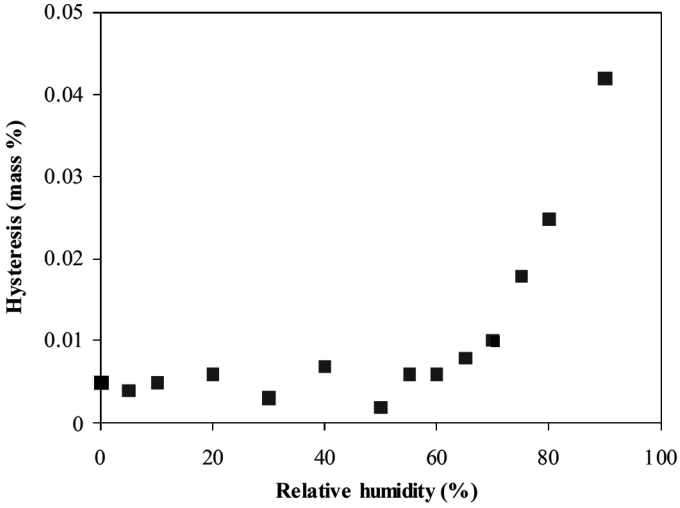


**FIGURE 11** Evolution of the hysteresis as a function of RH. The hysteresis increases significantly at RH greater than the critical RH for adhesion.



sorption-desorption isotherms occurred approximately in the same RH range as the abrupt loss in adhesion of PMMA to glass substrates. This supports the idea that water sorbed in the bulk PMMA is likely to have a strong impact on the adhesion loss of PMMA/glass joints at the critical RH.

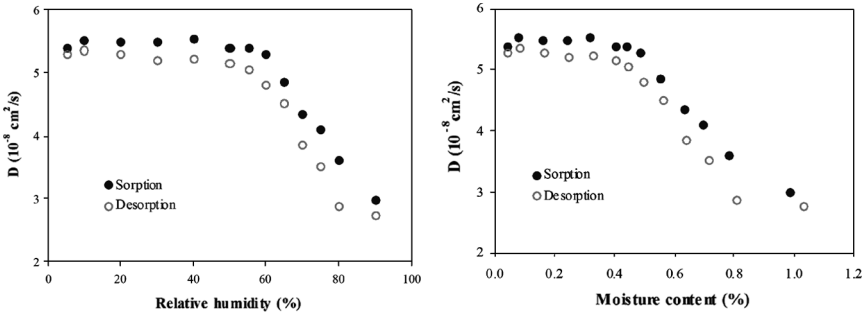


**FIGURE 12** (a) Evolution of diffusion coefficients at 23°C as a function of RH, and (b) as a function of moisture content. A decrease in the diffusion coefficient at higher water concentration is consistent with a clustering of moisture in the PMMA at high RH.

The GAB model has been used to obtain more details on the bulk sorption mechanism. Analysis of water isotherms by the GAB model has been shown suitable to describe BET Type III isotherms [33]. Experimental data for moisture sorption and desorption were used in determining the constants $C$, $m$, and $k$ in the GAB model from regression (Fig. 10). Curve-fitting efficiency is estimated from the residual sum of squares (RSS) defined by $RSS = \sum(m_{\text{exp}} - m_{\text{calc}})^2$, which shows a good fit between the experimental data and the model over the entire range of RH. The results of the GAB analysis on both sorption and desorption data of PMMA at 23°C are presented in Fig. 10. As already mentioned, the positive deviation from linearity, *i.e.*, from Henry's law, at high RHs and the concentration dependence of the diffusion coefficient may be ascribed to the clustering of water molecules. The clustering phenomenon occurs by water molecule association in the vicinity of water molecules sorbed to the polymer sorption sites. The number of water molecules in a cluster can be estimated from the GAB parameters and the volume fraction ($\varphi$), calculated as the ratio of the volume of sorbed water at the sorption and desorption equilibriums to the volume of dry polymer [36]. Values of $\varphi$ were determined from the moisture contents using a film density of $1.19\,\text{g/cm}^3$ (data from the manufacturer). The cluster number ($N_C$), represents the average of excess water molecules in the vicinity of a water molecule sorbed to the polymer including itself, and can be expressed as follows:

$$N_C = -(1-\varphi)\cdot\left[\frac{\varphi}{mc}\cdot(-2Cka_w + 2ka_w + C - 2) - 1\right]. \qquad (5)$$

Values of $N_C$ greater than 1 indicate the formation of water clusters. The results are reported in Fig. 13. For the sorption stage, there is no clustering effect at RHs below 50% since $N_C$ is equal to unity. The amount of water sorbed in the polymer results from random interactions between water molecules and sorption sites throughout the polymer. At higher RH, the number of water molecules in clusters increases as RH increases indicating water clustering is occurring. The water uptake can be then considered to be the sum of water sorbed by the polymer and water molecules involved in the formation of clusters. Cluster growth results from a higher affinity between water molecules than between water molecules and the PMMA. At 94.5%RH, clusters are composed of the association of an average of three water molecules. During the desorption stage, the amount of clustered water molecules decreases with decreasing the RH but values at a given RH are greater than for the sorption. Below

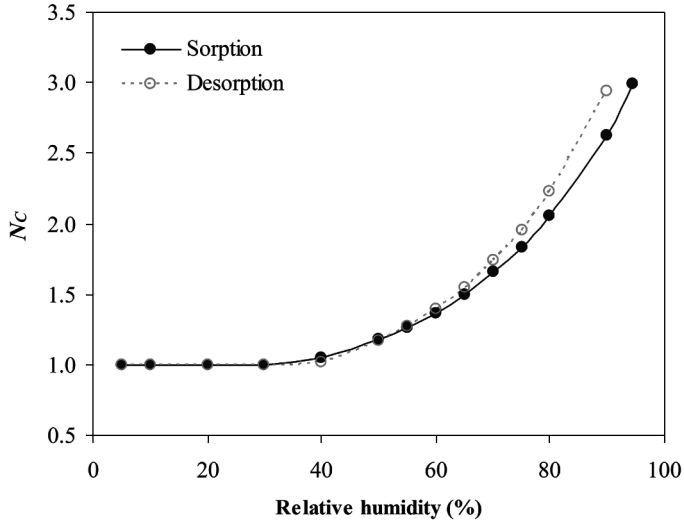


**FIGURE 13** Evolution of the number of water molecules per cluster as a function of RH for sorption and desorption as determined from the GAB model.



65%RH, curves for both sorption and desorption overlapped, coinciding with moisture content results mentioned earlier.

## 3.4. Mechanism of Failure

Based on the results presented above, there appear to be arguments for both interfacial and bulk effects in determining the critical RH for adhesion loss. To explore the question further, we turn to the fundamental nature of adhesion through a thermodynamic description. The intrinsic hydrolytic stability of the adhesive/substrate interface in the presence of an aqueous environment may be assessed from the thermodynamic arguments advanced by Gledhill and Kinloch [37]. The thermodynamic work of adhesion ($W_A$) was defined as:

$$W_A = \gamma_a + \gamma_s - \gamma_{as}, \tag{6}$$

where $\gamma_s$ and $\gamma_a$ are the surface free energies of the adhesive and substrate, respectively, and $\gamma_{as}$ is the interfacial surface energy between the substrate and adhesive. In the presence of liquid (denoted by the subscript '*l*'), this expression is defined by:

$$W_{AL} = \gamma_{al} + \gamma_{sl} - \gamma_{as}, \tag{7}$$

where $\gamma_{al}$ and $\gamma_{sl}$ are the interfacial surface free energies of the adhesive/liquid and substrate/liquid, respectively. Diiodomethane and distilled water were used as the test liquids, and the results are tabulated in Table 3. The values of $W_A$ between PMMA and the glass substrate in an inert environment and in the presence of moisture were found to be 91 and 7 $mJ/m^2$, respectively. These $W_A$ values in both environments indicate that the interface is significantly weakened in the presence of moisture but is relatively stable in both cases, *i.e.*, water can weaken the adhesion but is not capable of displacing the adhesive layer from the substrate. Such strong adhesion across the PMMA/glass interface is a result of strong acid-base interaction between basic ester carbonyl groups of PMMA and acidic surface silanols groups (Si−OH) on the glass *via* the formation of hydrogen bonds. Indeed, it is estimated that one to two silanol groups per square nanometre interact with the adsorbed PMMA, depending on the concentration of carbonyl groups near the glass surface and the distribution of the silanol groups [38]. Water molecules are too weak to compete effectively against the strong interfacial PMMA/glass acid-base bonds. This premise is consistent with the observations made in the present study in that cohesive failures within the PMMA layer were seen for the exposure up to 68% RH. Thus, based upon these calculations, a solely interfacial effect cannot be responsible for the presence of a critical RH for adhesion.

Because of the high electronegativity of oxygen compared with hydrogen, water molecules exhibit a strong dipole, and interact strongly with other charged or polar groups, such as silanol groups on glass substrate. For example, a glass surface exposed to typical ambient environments is hydrated by a network of water molecules that are hydrogen bonded to the silanol groups [29]. A multilayer of sorbed water could exist even at ambient temperature and humidities,



**TABLE 3** Contact Angles and Surface Free Energies for Glass and PMMA Surfaces

| | Contact angle (°) | | Surface free energy ($mJ/m^2$) | |
|---|---|---|---|---|
| | Distilled water | Diiodomethane | Dispersion component | Polar component |
| Water [1] | – | – | 22.0 | 50.2 |
| Diiodomethane [1] | – | – | 48.5 | 2.3 |
| Glass | $27.0 \pm 3.4$ | $43.2 \pm 1.0$ | 23.7 | 43.7 |
| PMMA | $73.3 \pm 1.8$ | $31.2 \pm 4.1$ | 38.9 | 5.9 |

which is attributed to the fact that hydrogen bonding between two or more water molecules is often energetically competitive with the molecule-substrate bond [39]. Water in close proximity to the glass surface is strongly bonded to silanol groups, and is difficult to remove even pumping in vacuum over extended periods of time at room temperature [40]. However, the adsorbed water on the glass surface may be removed by heating in a dry environment to $\geq 200^{\circ}C$ [41]. Since the glass substrates used here were not heat-treated prior to bonding, and complete cohesive joint failures within the PMMA layer were observed for exposure at the ambient condition, the presence of an initial amount of water on the glass surface would not interfere significantly with the adhesion of the PMMA/glass oxide interface, such that the interfacial bonds are still stronger than the cohesive strength of the bulk PMMA.

A rapid decrease in $G_C$ was observed at the critical RH region, and was accompanied by the positive deviation from Henry's law in the water sorption isotherm plot, as presented earlier. Such apparent correlation between the rapid adhesion loss and the equilibrium moisture content of the bulk polymer has led to a postulation that the mechanism governing the critical RH is a phenomenon attributed solely to the bulk polymer itself [17,26]. However, the loci of joint failure at the critical RH was established to be a complex failure path involving truly interfacial failure along the PMMA/glass oxide interface and cohesive failure within the PMMA layer. This observation indicates that the interface, which initially has greater interfacial adhesion strength than the cohesive strength of the bulk PMMA, becomes relatively weak upon exposure to moisture. Thus, an interfacially based phenomenon would be expected to play a crucial role in the adhesion loss at the critical relative humidity.

To assess the role of the interface, NR was used to quantify the moisture content at the interface. This critical piece of information has been lacking and, thus, it has been difficult to determine the mechanisms by which failure of the adhesive joint occur. NR shows that an accumulation of moisture at the PMMA/glass interfacial region is significantly greater than the bulk solubility of water in the PMMA. The amount of moisture near the interface is strongly dependent upon RH as illustrated in Fig. 14. These concentration profiles are for the water in the PMMA phase. We assume that no $D_2O$ is absorbed by the glass layer. Note that the water concentration in Fig. 14 is provided in terms of volume fraction of heavy water ($D_2O$) within the film, while Fig. 11 is in terms of mass % of $H_2O$ within the film. These can be related to each other if the specific volume of water within the film can be assumed and that there is no excess volume

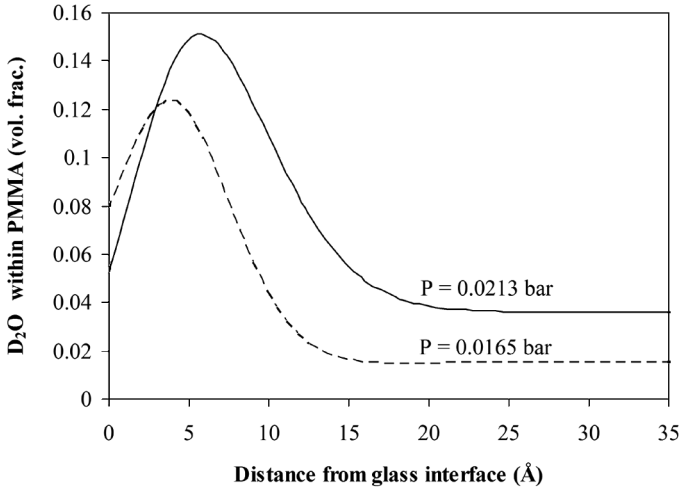


**FIGURE 14** Concentration profiles of $D_2O$ near the PMMA/$SiO_2$ interface as determined from NR. These concentrations are for the $D_2O$ within the PMMA phase. The interfacial excess increases with increasing partial pressure of $D_2O$, which is equivalent to increasing humidity.



upon mixing (regular solution theory). We have examined both thick (0.55 mm) and thin (15 μm) films of PMMA. The absolute solubility at a given RH does change slightly between the samples, but the trends in the data, including the discontinuity, are the same between the samples. Thus, the absolute solubility is dependent upon the processing for the PMMA, but the location of the solubility discontinuity is independent of processing. This latter property appears key to adhesion failure at the critical RH and, therefore, differences in the absolute solubility will not affect the interpretation of the data. Profiles were determined at a series of RH values, and the maximum water concentration near the interface is plotted in Fig. 15. The results show no discontinuity but rather a steady increase with RH even through the critical value for adhesion loss [42].

The origin of the adhesion loss at the critical RH, therefore, is postulated to be a combination of the physical changes in the bulk PMMA from moisture sorption and the displacement of the interfacial bonds by ingressing water molecules. It is well known that PMMA expands upon water sorption through relaxation of stresses induced by the osmotic pressure leading to swelling of the bulk polymer [43,44]. Swelling introduces localised stresses at the PMMA/glass oxide interface. This stress mismatch between the substrate and the constrained

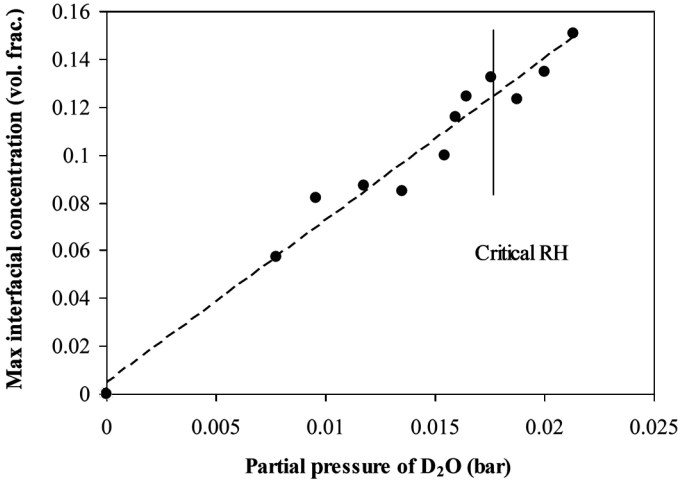


**FIGURE 15** Interfacial $D_2O$ concentrations determined using NR. A significant excess is observed near the interface that increases approximately linearly with humidity. Dashed line is provided as a guide to the reader. The critical RH is estimated from the discontinuity in the thickness of the PMMA film during exposure to $D_2O$ vapor.



polymer film upon swelling would weaken the interface, eventually leading to interfacial failure. Kinloch *et al*. [45] found that residual stresses induced at the adhesive/substrate interface from post-curing the adhesive (thermal stress) promote interfacial failure. Note that the stress state induced at the adhesive/substrate interface by swelling likely differs from the stresses introduced by the post-curing of adhesive. However, the presence of any mechanical stresses may increase the sensitivity of the adhesive/substrate interface to moisture attack. Further, the presence of high stresses at the crack tip may render interfacial bonds more susceptible to environmental attack by lowering the free energy barrier that must be crossed if the bond is to change from an unbroken state to a broken state. Namely, the displacement of interfacial bonds by water may be exacerbated by the simultaneous presence of mechanical stresses. Also, this stress-assisted mechanism would explain why the interfacial PMMA/glass bonds, which were predicted as being stable against moisture intrusion from the thermodynamic arguments, rupture upon exposure to high RH.

Evidence for this stress-assisted mechanism is present in the NR data. In examining the moisture profiles such as those in Fig. 14, a series of such profiles were measured and the widths at half height

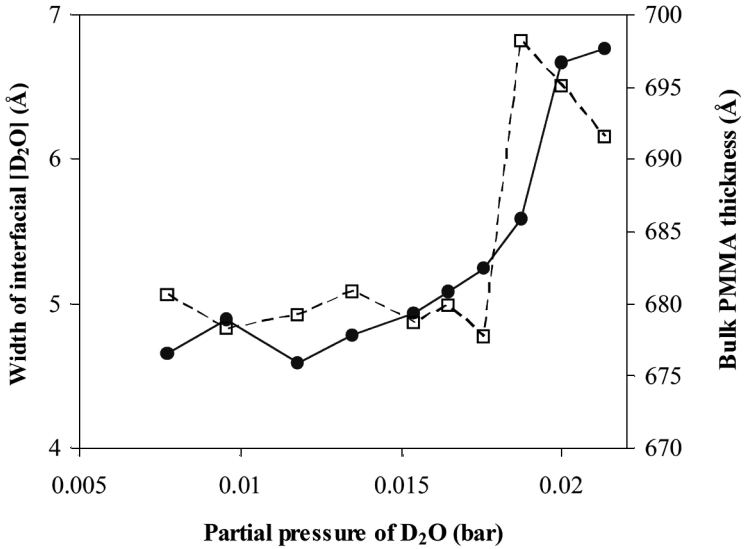


**FIGURE 16** The width of the $D_2O$ concentration excess near the oxide interface (●) as a function of the humidity. The width is nearly constant below the critical RH and then increases significantly above the critical RH. The thickness of the bulk PMMA layer (□) as determined by NR shows a discontinuity when the width of the interfacial excess of moisture increases.



are shown in Fig. 16 as a function of $D_2O$ partial pressure. The width is nearly invariant until the critical RH is reached at which point the width increases. The width of the interfacial water concentration increases significantly above the critical RH; this could be explained by stresses at the interface increasing the moisture content in the PMMA near the interface. To illustrate this more clearly the thickness of the bulk of the PMMA (not including any of the excess) is also shown in Fig. 16. Note the discontinuity in the thickness due to enhanced bulk solubility above the critical RH corresponds with the broadening of the interfacial water profile. Non-physical variation in the thickness results from the increase in the interfacial water content with increasing partial pressure that exceeds the bulk increase.

As evident from the NR data, multilayers of water accumulate at the PMMA/glass oxide interface with increasing RH. The presence of such layers at polymer/substrate interfaces has been well documented for structural adhesives as well as organic coatings [11,46–48], and has been attributed as the main cause for moisture-induced adhesion loss in many polymer/substrate systems. Indeed, the hydrogen bonds

between the first-layer water molecules and the silanol groups (about 25 kJ/mol), and the bonds between the first-layer and second-layer of water molecules (>40 kJ/mol) [49], are relatively weak. This water interphase is not capable of sustaining any stress, which accounts for the crack growth at extremely low values of $G_C$ and the truly interfacial nature of the failures along the PMMA/glass oxide interface at high RHs. Analogous to stress corrosion cracking phenomena, water uptake at the PMMA/oxide interface could also be enhanced by the swelling stresses. The interface, therefore, is further weakened by the presence of more water molecules, and the failure now occurs *via* failure of these broader discrete domains of water molecules near the interface. The interplay between bulk polymer swelling and the interface appears to be the critical factor in the adhesion loss at the critical RH.

It is noteworthy that the glass substrates used here consisted of a relatively small quantity of alkaline (sodium and potassium) oxides, which are extremely hygroscopic and, therefore, adsorb water. These alkaline oxides readily convert into hydroxides in the presence of water. The aggregation of hydroxides at the crack tip induces high pH excursions in the environs of the PMMA/glass oxide interface. Since PMMA is bonded to surface silanol groups on the glass oxide surface predominantly *via* acid-base interactions [50,51], the strong alkalinity of the PMMA/glass oxide interface upon moisture exposure would accelerate the hydrolysis of the interfacial bonds. In the present case, however, metal cations were not detected on the failure surfaces using the XPS. It is likely, therefore, that the concentrations of the alkaline oxides are too small to induce sufficient alkalinity and initiate the cathodic debonding mechanism. Furthermore, aluminium oxide and boric oxides on the glass surface may have compensated for the alkalinity of the hydroxides.

To shed more light on the failure mechanism, an adhesion loss recovery study was also conducted. In these experiments, adhesive joints were exposed for 3 days at 100% RH and subsequently dried for 720 h in desiccators at room temperature. Shaft-loaded blister tests were conducted to measure $G_C$ and the results are shown in Fig. 17. It can be seen that following drying of the joints, the values of $G_C$ recovered to some extent. The locus of joint failure changed from entirely interfacial failure along the PMMA/glass oxide interface to a complex failure path consisting of both cohesive failure in the PMMA layer and interfacial failure, which was confirmed by the XPS analyses (not shown). The recovery of adhesion upon drying is indeed consistent with the reversible effect of bulk swelling of PMMA in that desorption of water from the polymer matrix relieves the swelling stresses

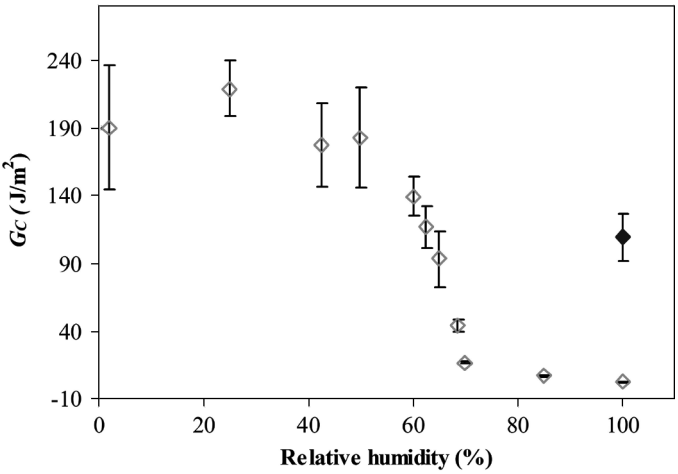


**FIGURE 17** Relationship between $G_C$ and the RH. Data denoted by the closed symbol was obtained from the adhesion recovery study. Only partial recovery of the strength of the joint is obtained after extended drying.



induced at the PMMA/glass oxide interface. It is apparent that not all adhesion strength is recovered, and it is reasonable to ascribe the irrecoverable component to irreversible interfacial bond rupture due to water attack. Also, it is likely that water is not completely removed after subsequent drying [52] as water molecules may strongly bond at the PMMA/glass oxide interface.

It should be noted that a simple interface, *i.e.*, between PMMA and glass, was used to understand the impact of moisture on adhesion. Due to the simplicity of this system, the extendibility of this model system to more structural interfaces is not obvious. However, many findings for more structural interfaces of critical RH [17,26] are consistent with the conclusions from this study.

## 4. CONCLUSIONS

The mechanism of sudden adhesion loss at a critical RH was examined for a model system of PMMA on glass. The adhesive fracture energies of these interfaces were determined using a shaft loaded blister test over a range of RH. There appears to be a critical concentration of water below which the environment has a minimal impact on the adhesion at a critical RH. A discontinuity in the moisture sorption isotherm in PMMA occurs at this critical RH, which is consistent with literature that attributes the critical RH effect to changes in the bulk

adhesive. Conversely, XPS and ATR-FTIR on the fracture surfaces illustrate failure above the critical RH is interfacial in nature between the PMMA and the glass. This result suggests the interface is closely related to the RH effect. To resolve this controversy, NR was utilized to quantify the moisture content in the PMMA/glass interfacial region. An excess water concentration above the bulk solubility in PMMA is observed near the interface. This concentration increases linearly with RH even through the critical RH. However, the width of the excess moisture in the interfacial region rapidly increases above the critical RH. A mechanism for loss of adhesion at a critical RH is proposed based upon water both producing stresses through swelling of the PMMA and reducing the strength of the PMMA/glass oxide interface. These effects are magnified by the fact that local concentration of water near the interface is significantly higher than that in the bulk PMMA.



## ACKNOWLEDGMENTS

The authors thank Dr. Tinh Nguyen of NIST and Prof. Tony Kinloch of Imperial College London for their valuable comments.

## REFERENCES

[1] Kinloch, A. J., *Adhesion and Adhesives: Science and Technology* (Chapman and Hall, London, 1987).
[2] Wylde, J. W. and Spelt, J. K., *Int. J. Adhesion Adhesives* **18**, 237–246 (1998).
[3] Bowditch, M. R., *Int. J. Adhesion Adhesives* **16**, 73–79 (1996).
[4] Su, N., Mackie, R., and Harvey, W., *Int. J. Adhesion Adhesives* **12**, 85–93 (1992).
[5] Sargent, J. P. and Ashbee, K. H. G., *J. Phys. D: Appl. Phys.* **14**, 1933–1938 (1981).
[6] Weitsman, Y., *J. Comps. Mater.* **11**, 378–394 (1977).
[7] Gazit, S., *J. Appl. Polym. Sci.* **22**, 3547–3558 (1978).
[8] Xiao, G. Z. and Shanahan, M. E. R., *J. Polym. Sci., Part B: Polym. Phys.* **35**, 2659–2670 (1997).
[9] Loh, W. K., Crocombe, A. D., Abdel Wahab, M. M., Watts, J. F., and Ashcroft, I. A., *J. Adhesion Sci. Technol.* **16**, 1407–1429 (2002).
[10] Kinloch, A. J., Korenburg, C., Tan, K. T., and Watts, J. F., *J. Mater. Sci.* **42**, 6353–6370 (2007).
[11] Nguyen, T., Byrd, E. W., Bentz, D., and Martin, J., *J. Adhesion* **81**, 1–28 (2005).
[12] Venables, J. D., *J. Mater. Sci.* **19**, 2431–2453 (1984).
[13] Brewis, D. M., Comyn, J., Raval, A. K., and Kinloch, A. J., *Int. J. Adhesion Adhesives* **10**, 247–253 (1990).
[14] Kalashnikova, I. V., Matveev, V. V., and Arslanov, V. V., *Colloid J.* **58**, 722–729 (1996).
[15] Watts, J. F., *J. Adhesion* **31**, 73–85 (1989).
[16] Watts, J. F. and Castle, J. E., *J. Mater. Sci.* **19**, 2259–2272 (1984).

[17] Lefebvre, D. R., Takahashi, K. M., Muller, A. J., and Raju, V. R., *J. Adhesion Sci. Technol.* **5**, 201–227 (1991).
[18] Cognard, J., *Int. J. Adhesion Adhesives* **8**, 93–99 (1988).
[19] Xiao, G. Z., and Shanahan, M. E. R., *Polymer* **39**, 3253–3260 (1998).
[20] Wan, K. T. and Mai, Y. W., *Int. J. Frac. Mech.* **74**, 181–197 (1995).
[21] O'Brien, E. P., Case, S. L., and Ward, T. C., *J. Adhesion* **81**, 41–58 (2005).
[22] Wunderlich, W., in *Polymer Handbook*, J. Brandrup, E. H. Immergut, and E. A. Grulke (Eds.) (Wiley-Interscience, New Jersey, 1999). 4th ed., pp. V87–V90.
[23] Colthup, N. B., Daly, L. H., and Wiberley, S. E., *Introduction to Infrared and Raman Spectroscopy* (Academic Press, New York, 1990).
[24] Jonquieres, A. and Fane, A., *J. Appl. Polym. Sci.* **67**, 1415–1430 (1998).
[25] Maggana, C. and Pissis, P., *J. Polym. Sci, Part B: Polym. Phys.* **37**, 1165–1182 (1999).
[26] Lefebvre, D. R., Elliker, K. M., Takahashi, K. M., Raju, V. R., and Kaplan, M. L. *J. Adhesion Sci. Technol*. **14**, 925–937 (2000).
[27] Kinloch, A. J., *J. Adhesion* **10**, 193–219 (1979).
[28] Gledhill, R. A., Kinloch, A. J., and Shaw, S. J., *J. Adhesion* **11**, 3–15 (1980).
[29] Iler, R. K., *The Chemistry of Silica: Solubility, Polymerization, Colloid and Surface Properties, and Biochemistry* (Wiley-Interscience, New York, 1979).
[30] Nguyen, T. and Byrd, W. E., *Proceedings of the 11th International Conference in Organic Coatings Science and Technology*, (1987), pp. 178–190.
[31] Ernsberger, F. M., *Annu. Rev. Mater. Sci.* **2**, 529–572 (1972).
[32] O'Brien, E. P., White, C. C., and Vogt, B. D. *Adv. Eng. Mater.* **8**, 114–118 (2006).
[33] Brunauer, S., *The Adsorption of Gases and Vapours* (Princeton University Press, Princeton, NJ, 1943).
[34] Schult, K. A. and Paul, D. R., *J. Polym. Sci., Part B: Polym. Phys.* **34**, 2805–2817 (1996).
[35] Crank, J. and Park, G. S., *Diffusion in Polymers* (Academic Press, New York, 1968).
[36] Chin, J., Forster, A., Clerici, C., Sung, L., Oudina, M., and Rice, K., *Polym. Degrad. Stab.* **92**, 1234–1246 (2007).
[37] Gledhill, R. A. and Kinloch, A. J., *J. Mater. Sci. Letters* **10**, 1261–1263 (1975).
[38] Berquier, J. M. and Arribart, H., *Langmuir* **14**, 3716–3719 (1998).
[39] Bowden, F. P. and Throssell, W. R., *Nature* **167**, 601–602 (1951).
[40] Thiel, P. A. and Madey, T. E., *Surf. Sci. Rep.* **7**, 211–385 (1987).
[41] Zhuravlev, L. T., *Colloid Surf. A* **74**, 71–90 (1993).
[42] Tan, K. T., Vogt, B. V., White, C. C., Steffens, K. L., Goldman, J., Satija, S. K., Clerici, C., and Hunston, D. L., to be submitted.
[43] Souder, W. and Paffenbarger, G. C., *Physical Properties of Dental Materials*, National Bureau of Standards, Circular No. C433, Washington, D. C., 1942.
[44] Turner, D. T., *Polymer* **23**, 197–202 (1982).
[45] Kinloch, A. J., Thrusabanjong, E., and Williams, J. G., *J. Mater. Sci.* **26**, 6260–6270 (1991).
[46] Wu, W.-L., Orts, W. J., Markrzak, C. J., and Hunston, D. L., *Polym. Eng. Sci.* **35**, 1000–1004 (1995).
[47] Bascom, W. D., *J. Adhesion* **2**, 161–183 (1970).
[48] Leidheiser, H. and Funke, W., *J. Oil Color Chem. Assoc.* **70**, 121–132 (1987).
[49] Klier, K., and Zettlemoyer, A. C., *J. Colloid Interf. Sci.* **58**, 216–229 (1977).
[50] Fowkes, F. M., in *Physicochemical Aspects of Polymer Surfaces*, K. L. Mittal (Ed.) (Plenum Press, New York, 1981), pp. 583–603.
[51] Watts, J. F., Leadley, S. R., Castel, J. E., and Blomfield, C. J., *Langmuir* **16**, 2292–2300 (2000).
[52] Kent, M. S., McNamara, W. F., Fein, D. B., Domeier, L. A., and Wong, A. P. Y., *J. Adhesio*n **69**, 121–138 (1999).